MULTIFUNCTIONAL COMPOSITES WITH APPLICATIONS TO ENERGY PERFORMANCE AND EFFICIENCY

J. P. Thomas[1*], M. H. Merrill[1], K. M. Metkus[2], A. Piqué[3], and R. K. Everett[4]
[1] Multifunctional Materials Branch, Code 6350; [3] Materials and Sensors Branch, Code 6360;
[4] Materials Science Division, Code 6300
Naval Research Laboratory (NRL), Washington, DC 20375, USA
[2] NOVA Research, Inc., Alexandria, VA
(*Corresponding Author: james.p.thomas@nrl.navy.mil)

Keywords: *poro-vascular, electrode-wetting-on-dielectric, ionic liquid, hydrophobic, drag.*

1 Introduction

Multifunctional material systems (MfMS) are material/systems that can perform more than one "primary" function simultaneously or sequentially in time to enhance system-level performance through the elimination of redundancy between sub-system materials and functions.

A system-level performance metric of considerable importance is energy performance and efficiency. Total energy usage in 2009 by US Department of Defense (DoD) has been estimated at ~900 trillion BTU's with approximately 75% of that being consumed for mobility related applications (e.g., aircraft, ships, vehicles, etc.) [1]. This is the equivalent of 5.7 billion gallons of gasoline.

A key factor for energy waste in mobility applications is the aero/fluid-dynamic drag, which is generally comprised of skin-friction and form (or pressure) components. To maintain a steady-state velocity, the propulsion system must supply power equal to the drag force times the vehicle velocity. This is a direct waste of energy, and it does not include system propulsion losses. Technologies affecting drag offer opportunities for improving system-level energy efficiencies and performance.

This paper describes the development of a new class of multifunctional laminate composites with controllable surface morphology at NRL. The current focus is on two-phase (solid-fluid), thin, flexible, skin-like laminates with surface "pore" arrays that are connected to an internal vascular network. These new materials with structural (skin) + surface (morphology control) multifunctionality are being called "poro-vascular composites" or PV composites for short.

The PV structural skins are being developed with an ionic liquid (IL) phase whose height and meniscus shape within the pores can be controlled to vary the meso-scale surface morphology from dimples to domes (see Figure 1). IL's are neutral mixtures of charged (+ and -) species that exhibit very low vapor pressures [2]. Surface morphology directly affects skin-friction drag and indirectly affects form drag through the location of the laminar-to-turbulent transition point on the surface. IL control (height and meniscus shape) is achieved through manipulation of liquid capillary physics and Electrode-Wetting-On-Dielectric (EWOD) phenomena.

Currently available research results are reported following a summary of relevant background on surface roughness effects on fluid-dynamical drag and EWOD phenomenology. The paper concludes with a summary and suggested future research.

2 Background

Surface morphology directly influences skin-friction drag. It also influences form drag through its effect on the critical Reynolds (*Re*) number for transition from laminar to turbulent flow, which demarcates flow separation and a consequent decrease in the fluid-surface normal pressure [3]. Kithcart & Klett [4] show that ~1-3x increases in skin-friction drag and heat transfer are possible on flat plates with hemispherical dimples and protrusions in the turbulent boundary-layer, and that dimples are more effective than protrusions for enhancing the heat-transfer with minimal skin-friction drag penalty.

Electrode-Wetting-On-Dielectrics (EWOD) is a method for effecting changes in apparent contact angle of liquids on insulated solid surfaces with applied electrical field [5]. Figure 2 shows a generic flat EWOD configuration made with materials of specific interest to this work. The substrate is a thin layer of polyimide (Kapton ~100's μm). A layer of

conductive gold (~100 nm) or other metal(s) is vapor-deposited followed by vapor-deposition of dielectric Parylene (HT or C; ~μm) polymer. On the surface, a thin layer of Teflon AF (~200 nm) is spin-coated for hydrophobicity. Small drops of ionic liquids in contact with a conductive probe are polarized to create an electric field between probe and substrate. On the schematic plot in Figure 2, at zero applied potential, the hydrophobic coating produces a non-wetting state (contact angle > 90 deg). As the potential is increased, the contact angle decreases. A saturation regime is reached where the contact angle no longer decreases with increasing polarization [5]. Hysteresis between an advancing and receding contact angle is also typical.

3 Methods

3.1 System Modeling and Design

System-level design of the PV composites starts with a first-order model of the liquid-pore system that relates meniscus shape and height with pore diameter, contact angle, and liquid surface tension. The model is developed utilizing the equations of Laplace-Young and Lippmann-Young (below), and geometric relations.

The dimensionless Bond number is the ratio of gravity forces to surface tension forces in a liquid sample in contact with another phase [5,6]:

$$B_0 = \frac{\Delta\rho g l}{\gamma / l} \tag{1}$$

where $\Delta\rho$ is the density difference between the liquid of interest and the other phase (e.g., air), g is the acceleration of gravity, l is a characteristic length (e.g., pore diameter), and γ is the surface tension. Using the properties of water and assuming pores ~1 mm in diameter gives $B_0 \sim 0.1$. This implies that gravity is not a significant factor in the PV composites fluid mechanics and can be ignored.

In the absence of gravity and considering only circular pores, the Laplace-Young equation for pressure jump across the fluid meniscus is [5,6]:

$$\Delta P = \left(P_{liq} - P_{atm}\right) = \frac{2\gamma}{r} \tag{2}$$

where r is the radius of curvature (spherical).

In the pre-saturation region, the relation between contact angle and applied potential is given by the Lippmann-Young equation (Eq. 8 of [5]):

$$\cos\theta = \cos\theta_0 + \frac{\varepsilon_0 \varepsilon}{2t\gamma} V^2 \tag{3}$$

where θ is the contact angle, θ_0 is the zero-potential contact angle, ε_0 is the permittivity of vacuum, ε is the insulator dielectric constant, t is the insulator thickness, γ is the liquid's surface tension, and V is the applied potential.

The following relations are derived using Eqs. (2) and (3) and geometric relations to obtain equations for the "gage" pressure, ΔP, and meniscus height, h:

$$\Delta P = \frac{-4\gamma}{d}\cos\theta \tag{4}$$

$$h = \frac{d}{2}\left(\frac{\sin\theta - 1}{\cos\theta}\right) \tag{5}$$

where γ is the surface tension, d is the pore diameter, and θ is the fluid-solid contact angle measured from the capillary wall. These equations are used to generate plots of ΔP versus height h for various contact angles in the next section.

Pore-channel prototypes (50 x 75 mm) were fabricated and tested to provide support for the above modeling results and to provide understanding for the effects of different liquid flow rates, viscosity, etc. on fluid control in PV composites. Prototypes were laser micro-machined out of polyetherimide (Ultem) or polyimide (Kapton). Channel configuration effects on the supply of water or isopropanol (IPA) to multiple pores under slow and quasi-static flows was investigated. Linear designs consisting of straight channels with in-line pores were compared with fractal designs having multiple branched channels. Two linear (in-line pores) and two fractal (equi-distant pores) channel-pore prototypes with eight pores, 100 μm or 500 μm diameter, were fabricated and tested.

3.2 Materials and fabrication

Kapton and Ultem layers were bonded together to create the solid-phase PV composite components. Kapton HN with gold, silver, or copper conduction coatings and conductive Kapton RS or XC were selected for the pore layers. Kapton HN or FN (with an integral Teflon fluoropolymer FEP heat-sealing layer) and Ultem were selected for the network layers. Pyralux acrylic adhesive or the integral heat fluoropolymer heat seal (Kapton FN) were selected for bonding the various layers. Three PV composite

laminate design configurations were studied to assess ease of fabrication (Figure 3).

Subtractive Laser-Direct-Write (LDW) [7] with a pulsed UV laser (266 nm) was used for micro-machining arbitrary shaped pores, various pore arrays, and different sized (width and depth) vascular trenches or channels in a variety of polyimide and polyetherimide materials. The laser spot-size used (15-25 μm) allowed for features as small as 50 μm to be machined. Characterization of machining precision is ongoing in terms of metrics such as pore circularity and cylindricity, trench cross-section squareness, feature positional tolerances, and resultant surface finishes.

Additional dielectric and hydrophobic coatings must be applied on the conducting pore layer for EWOD (see Figure 4). The dielectric coating is ideally thin, pinhole-free, conformal, and extends into the pores covering all conductive surfaces. Parylene-HT and Parylene-C in thicknesses ranging from 500 nm to more than 10 μm have been selected for this purpose. The hydrophobic coating increases the (non-polarized) contact angle to a value greater than 90 degrees (non-wetting). Teflon AF 1600 (Dupont), an amorphous fluoropolymer that can be dissolved in select solvents for spin-coating, was chosen for this purpose. Teflon AF films with thicknesses in the 100-200 nm range and a roughness (Ra) less than ~1 nm (on a silicon substrate) were spin-coated using 1% to 2% solutions by weight. The resulting contact angle for water drops was 110 to 115 degrees (advancing) with minimal hysteresis (less than 10 degrees).

Six commercial IL's were selected based on their sub-ambient (<RT) solidification points, non-hygroscopic tendencies, and low-toxicity. Their densities ranged from 867 to 1240 kg/m^3, and their surface (interfacial) tension values, measured as part of this work, ranged from 24 to 53 mN/m.

3.3 Liquid Shape Control

A fully electroded flat EWOD sample was prepared for proof-of-concept demonstrations. A Kapton 200EKJ film was coated with ~150 nm of Au, a 10 μm coating of Parylene-HT, and a 200 nm (nom) layer of Teflon AF 1600. For the demonstration, 1 μL of 1-ethyl-3-methylimidazolium acetate IL (IFT = 43 mN/m) was deposited on the surface, and voltage was applied in steps of 25 V up to 200 V with a 4 second pause after each step.

3.4 Characterization

An FTA 1000 Drop-Shape Characterization System was used to measure liquid surface (interfacial) tensions of the IL's and liquid-solid contact angles. Surface tensions were measured using a pendant drop method, and contact angle were measured using small (1-5 μL) sessile drops. By pumping liquid in and out of the drop, both advancing and receding contact angles were measured. For EWOD, a Keithley 2400 Source Meter was used for voltage control, and LabView was used to coordinate and synchronize the voltage control with voltage/current data collection and drop shape videography. Post-test analysis of the contact angles with the FTA software provided contact angle values at each step.

Surface morphologies were measured using a JEOL variable pressure SEM at high vacuum, a Veeco Dimension 3100 Scanning Probe Microscope in tapping mode, and a Lext OLS 3000 Confocal Laser Scanning Microscope. Surface roughness (Ra) and film thickness were measured using a KLA Tencor P10 stylus profilometer with a 2 μm stylus, 0.5 mg load, and picometer height resolution. Coating roughness and thickness data refers to films deposited on smooth silicon wafer substrates. This provides a very consistent surface for comparing the effects of processing. Parylene/Teflon AF adhesion was measured using a modified tape test. Samples were razor cut (3-6 lines, 2 mm spacing) at 0 and 90 degrees to the tape-pull direction. SEMicro CHT tape (synthetic rubber adhesive, 12 to 25 mm wide x 75 mm long) was firmly pressed onto the testing area, allowed to sit for 90+/- 30 sec, and then rapidly removed by pulling the tape directly back on itself (180 deg). The fraction of debond area 'quantifies' the quality of the Teflon AF adhesion.

4 Results and Discussion

4.1 System design

Figure 5 shows plots of pressure vs. height for contact angles ranging from 50 to 140 degrees. Control regime A-B on the gray curve (θ = 50 deg) corresponds to a rise of fluid in the pore with constant curvature (pressure), which is controlled by the contact angle of liquid on the pore wall. At point B, the fluid just reaches the upper edge of the pore exit. As the fluid continues to fill the pore, it "bulges" on the surface corresponding to an apparent

change in contact angle and curvature. At point C, the apparent contact angle has increased from θ to $\theta + \pi/2$, as measured from the pore wall, or from $\theta' - \pi/2$ to $\theta' = \theta$ relative to the exterior surface. Beyond point C (to D), the liquid spreads on the surface while maintaining its contact angle and spherical shape. It grows in height (volume) with a corresponding increase in radius of curvature and consequent decline in pressure.

Liquids with contact angles ≥ 90 deg will reach point E, which corresponds to the maximum possible pressure (minimum curvature). At this point, the apparent contact angle is 180 deg relative to the pore wall (i.e., parallel). Continued filling leads to an increase in height and radius of curvature and a consequent decline in pressure.

Simultaneous control of contact angle and fluid volume in the pore is required to achieve a full range of morphology control (dimpled to domed). The applied potential controls the contact angle, and displacement-pumping within the network controls the pore-fluid volume. The pressure is simply a response that develops as a consequence of the drop's curvature.

With multiple pores, there is a potential for unstable liquid spreading if the pressure in any single pore exceeds the maximum pressure point on the plot (e.g., point C or E). The maximum pressure is related to pore diameter, so it is important that fluidically connected pores have the same diameter.

The pore-channel prototype tests support these modeling conclusions. For example, regardless of channel geometry or pore size, the channel(s) consistently fill before any liquid exits the pores. A positive and increasing pressure is required for a liquid to bulge from a pore, hence the channels are disposed to filling first. After the channel is filled, fluid bulges from all the pores until one drop begins to spread. This creates an unstable state with the pressure decreasing as the drop spreads and the others shrink by "surface tension siphoning." No difference has been observed between the linear and channel arrays for slow fluid flows; this might have been expected given the quasi-hydrostatic network flow regime.

4.2 Materials and fabrication

A wide variety of pore, array, and channel-like features were laser micro-machined into the polyimide and polyetherimide materials. Figure 6 shows examples of the range of capabilities. Pores of arbitrary shape and size, pore-arrays with arbitrary sizes, arrangements, and spacings, and blind or through channels of various sizes and planar layouts were demonstrated. The least number of machining steps/time and the best pore-channel alignment precision were obtained with Configuration #3 (Fig. 3 (B)), which combines the pores and the network channels within one material layer which is then capped by the integrated adhesive/substrate layer. Measurements are ongoing to quantify dimensional tolerance limits and surface roughness characteristics for the various laser micro-machined features.

Surface characterization following Parylene-HT coating uncovered a unique roughness morphology (Figure 7). These images corresponded to a 12.2 μm thick coating of Parylene-HT on Kapton 200RS100 (conductive). An apparent multi-scale "granular" morphology developed, which may indicate localized nucleation of Parylene polymerization with subsequent growth and coalescence. Subsequent testing showed evolution of surface morphology during coating. The initial roughness (Ra) for plain Kapton HN film was 27 nm; after plasma etching and coating with a 12.2 μm thick Parylene-HT layer, the roughness increased to 80 nm; after coating with 200 nm of Teflon AF, the roughness decreased to 10 nm with a more 'wavy' profile. The modified tape pull-off test showed good adhesion (< 5% material removal) after plasma etching the Parylene surface prior to Teflon AF coating and thermal curing.

Results of the EWOD tests are shown in Fig. 8. The zero-voltage contact angle is 93+/-2 degrees, which is consistent with the lower surface tension of the IL relative to water (i.e., 72 mN/m vs. 43 mN/m). In the 0-125 V range, expected Lippmann-Young behavior is observed with a total decrease in contact angle of 20 degrees. On increasing the voltage from 125 to 200 V and then back to 100 V, the drop began 'scooting' around and the contact angle varied from 70 to 90 degrees. The current was very small, so dielectric breakdown did not occur. It may simply be a reflection of saturation, but the large hysteresis and swings in value are not typical of this behavior. The drop motion may be due to non-uniformities in surface roughness and dielectric coating thickness, which would result in a non-uniform contact angle and unpredictable lateral forces. Unintentional

surface debris may also be pinning the liquid. Research to identify and remedy this anomalous behavior is in progress. As the potential dropped below 100 V, the behavior was again Lippmann-Young with very little hysteresis between the initial and final contact angles.

5 Summary and Future Work

A new class of multifunctional laminate composites called "poro-vascular" composites with controllable surface morphology is being developed. Progress to date includes: 1.) formulation of a first-order model for fluid control with key design parameters identified and experimental data for support. The model shows that both contact angle and fluid volume control are necessary to achieve an extended range of surface morphologies; 2.) development of a feasible EWOD electrode system and fabrication method for PV composites. This is based on a two-layer laminate that allows for integration of complex features in an efficient process; 3.) proof-of-concept demonstration of EWOD control of an ionic liquid's contact angle (shape) on a flat sample with PV composite relevant materials and fabrication.

Future work will focus on the development of more advanced PV composite prototypes, improvement in EWOD performance with verification in glass capillaries as single-pore analogs, and computational modeling of boundary layer flows on PV composites with relevant surface morphologies and higher-order representations of EWOD fluid shape control.

6 Acknowledgements

This work was funded by Office of Naval Research (ONR).

7 Figures

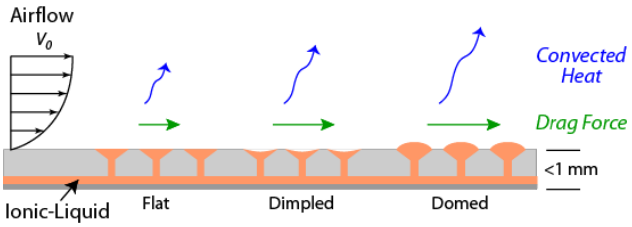

Fig. 1. PV composite surface morphologies for active control of drag and heat convection.

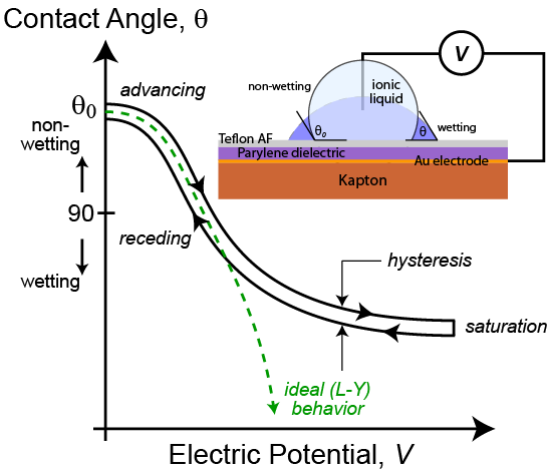

Fig. 2. Configuration for the flat layer Electrode-Wetting-On-Dielectric (EWOD) experiments, and contact angle vs. applied potential behavior. Ideal Lippmann-Young behavior given by Eq. (3).

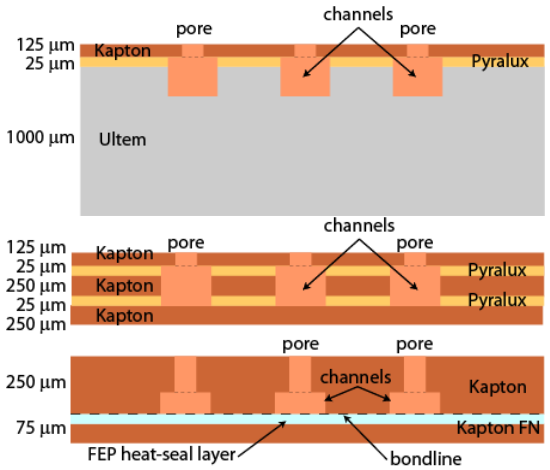

Fig. 3. Three PV composite designs. Design #3 (B) is simplest with the fewest machining operations.

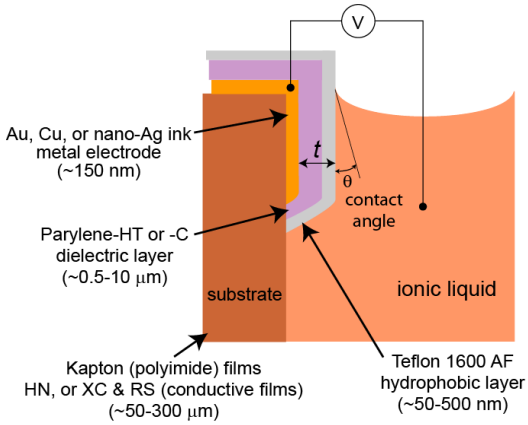

Fig. 4. Electroding for EWOD control contact angles in PV composites at the surface and within the pore.

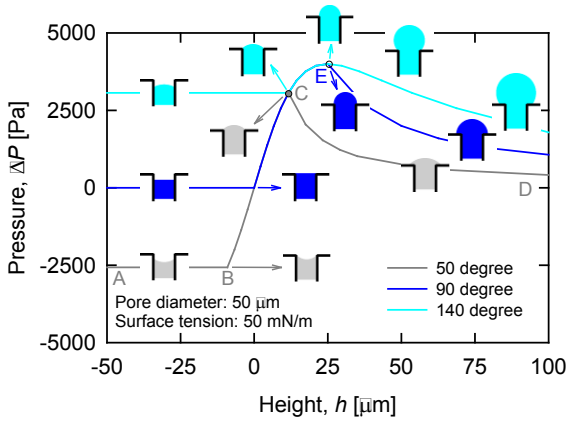

Fig. 5. Pressure versus height (relative to surface) with corresponding meniscus shapes for three contact angles (50-140 degrees).

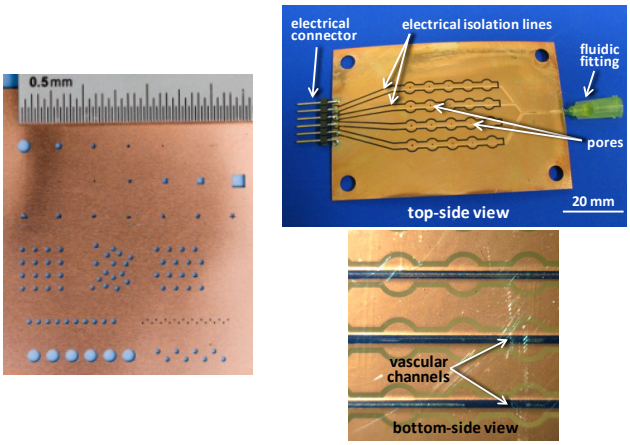

Fig. 6. (L) Cu-coated Kapton sample with various pore shapes and configurations; (T-R) An early PV composites prototype (75 x 50 mm); and (B-R) back view of the top sample showing vascular channels.

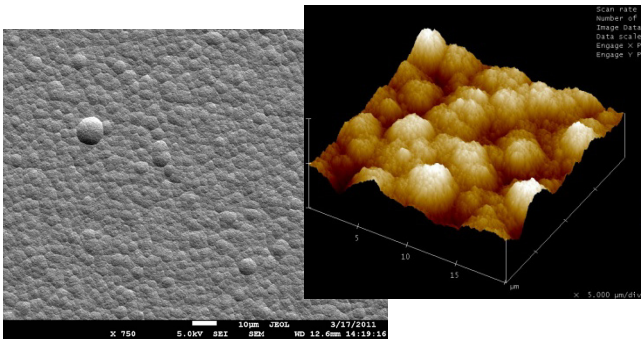

Fig. 7. L: SEM (scale bar = 10 μm) and R: AFM (20 x 20 μm region) images of a conductive Kapton surface showing granular morphology at two scales.

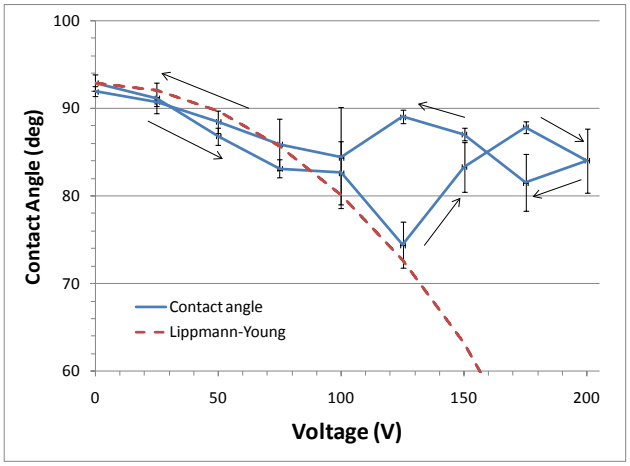

Fig. 8. EWOD results for a 1-ethyl-3-methylimidazolium acetate IL on Kapton HN - Parylene-HT (10.5 μm) - Teflon AF (200 nm). The arrows show progression of data with time.

8 References

[1] B. D. Craig, R. A. Lane, S. L. Knoeller, O. R. Conniff, C. W. Fink, and B. J. Ingold, "DoD Energy Handbook: Alternative and Renewable Energy Options for DoD Facilities and Bases, Spiral 2". *AMMT-38,* AMMTIAC, Rome, NY, 421 pgs., 2011.

[2] K. E. Johnson, "What's an Ionic Liquid?". *The Electrochemical Society Interface*, pp. 38-41, Spring 2007.

[3] B. R. Munson, D. F. Young, and T. H. Okiishi, "Fundamentals of Fluid Mechanics". Wiley, NY, 1990.

[4] M. Kithcart and D. Klett, "Heat transfer and skin friction comparison of dimpled versus protrusion roughness". *J. Enhanced Heat Transfer*, Vol. 3, pp. 273-280, 1996.

[5] F. Mugele and J-C. Baret, "Electrowetting: from basics to applications". *J. Phys. Condens. Matter*, Vol. 17, pp. R705-R774, 2005.

[6] A. W. Adamson and A. P. Gast, " Physical Chemistry of Surfaces". Wiley, NY, 1997.

[7] A. Piqué, R. Auyeung, H. Kim, K. Metkus and S. Mathews, "Digital microfabrication by laser decal transfer". *J. Laser Micro/Nanoeng.*, Vol. 3, pp. 163-169, 2008.